On the Evolution of
U.S. Temperature Dynamics

Francis X. Diebold   Glenn D. Rudebusch

University of Pennsylvania   FRB San Francisco

July 14, 2019

Abstract: Climate change is a multidimensional shift. While much research has documented rising mean temperature *levels*, we also examine range-based measures of daily temperature *volatility*. Specifically, using data for select U.S. cities over the past half-century, we compare the evolving time series dynamics of the average temperature level, AVG, and the diurnal temperature range, DTR (the difference between the daily maximum and minimum temperatures at a given location). We characterize trend and seasonality in these two series using linear models with time-varying coefficients. These straightforward yet flexible approximations provide evidence of evolving DTR seasonality, stable AVG seasonality, and conditionally Gaussian but heteroskedastic innovations for both DTR and AVG.

Key words: DTR, temperature volatility, temperature variability, climate modeling, climate change

JEL codes: Q54, C22

Contact: fdiebold@upenn.edu, glenn.rudebusch@sf.frb.org

1   Introduction

Climate change can be defined as the variation in the joint probability distribution describing the state of the atmosphere, oceans, and fresh water including ice (Hsiang and Kopp, 2018). These are complex, multidimensional physical systems, and the various features of climate change have been described using a diverse set of summary statistics. One of the most important aspects of climate change is the evolving distribution of temperature, and many subsidiary indicators have been used to measure this variation, including, for example, mean temperature, temperature range, hot and cold spell duration, frost days, growing season length, ice days, heating and cooling degree days, and start of spring dates (Masson-Delmotte et al., 2018; Reidmiller et al., 2018). Of course, the *level* of temperature – the central tendency of the distribution – has attracted the most attention, in particular, regarding the upward trend in the average daily temperature (AVG). In contrast, less attention has been given to temperature *volatility*, which can be measured by the diurnal temperature range (DTR), which is the difference between the daily maximum temperature (MAX) and minimum temperature (MIN) at a given location.

Similar to changes in temperature averages, changes in temperature ranges and variability can also have important effects on environmental and human health (Davy et al., 2017). For example, the incidence of temperature extremes such as heat waves depends critically on how the whole distribution of temperature is shifting – including both the central tendency and variability. Of course, such temperature extremes can have notable adverse effects on society and the economy. Temperature variability can stress workers and lower labor productivity, but it can also have direct effects on output. A salient example is agriculture, whose output is a function of capital, labor, and weather inputs.[1] Indeed, the very viability of certain agricultural sub-industries, notably wine or maple syrup production, is crucially dependent on temperature ranges. For example, Robinson (2006) notes that

> Diurnal temperature variation is of particular importance in viticulture. Wine regions situated in areas of high altitude experience the most dramatic swing in temperature variation during the course of a day. In grapes, this variation has the effect of producing high acid and high sugar content as the grapes' exposure to sunlight increases the ripening qualities while the sudden drop in temperature at night preserves the balance of natural acids in the grape.   (p. 691)

---

[1]Wigglesworth (2019) finds an important role of DTR in a panel study of U.S. state-level agricultural production over and above standard covariates like capital, labor, and AVG.

To better understand the full nature of the changing distribution of temperature, we examine DTR in select cities in the United States over the past half-century, quantifying both conditional-mean and conditional-variance dynamics. Our contribution is importantly methodological as we characterize the trend and seasonality in DTR using linear models that are easy to interpret but also quite adept at accounting for variation in the temperature distribution. We allow for time-varying coefficients, which provide a straightforward yet flexible approximation to more general nonlinear effects. Although our focus is on DTR, we also provide a parallel analysis for AVG, which allows valuable interpretive context and contrast. Our work reveals an *evolving* DTR conditional mean seasonal pattern, in contrast to the fixed AVG conditional mean seasonal pattern. In addition, our work reveals clear seasonality in conditional *variance* dynamics, both for DTR and AVG, although the evidence is weaker as to their evolution.

The previous research literature that examined DTR struggled for some time to develop firm conclusions about the dynamics of temperature variability. Even the direction of the trend in DTR has been somewhat contentious (Alexander and Perkins, 2013). Recent work has established that the downward trend in DTR in many locations reflects a more rapid warming of MIN than MAX – generally the result of nighttime lows rising faster than daytime highs (Davy et al., 2017). However, this differential trending of MIN and MAX, or "diurnal asymmetry," is not geographically uniform because of variation in vegetation, cloud cover, and other factors (Jackson and Forster, 2010; Sun and Pinker, 2014). Along with this trend in temperature variability, seasonal variation in DTR has also been considered by a few authors, including Ruschy et al. (1991) and Durre and Wallace (2001), who describe a lower temperature range in winter than at other times. Qu et al. (2014) also provide some evidence that the seasonality of DTR in the United States may be changing over time. To capture as much variation as possible in the distribution of DTR – including trend and seasonal – we use linear time series models with time-varying coefficients to provide simple yet powerful representations.

We proceed as follows. In section 2, we provide an introductory analysis for a representative city, Philadelphia. Then, in section 3, we broaden the analysis to include fifteen geographically dispersed U.S. cities, characterizing both conditional-mean and conditional-variance dynamics. We conclude in section 4.

Figure 1: Estimated Densities, AVG and DTR, Philadelphia
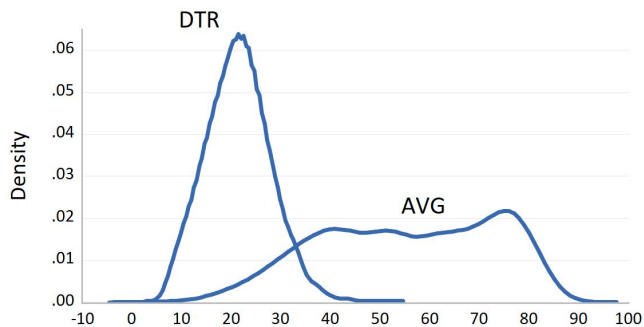
Notes to figure: We show kernel density estimates for daily AVG and DTR, 1960-2017.

2   Philadelphia

We introduce and illustrate our approach by studying temperature data measured at the
Philadelphia airport (PHL) in a step-by-step fashion. We present most results graphically,
while regression results on which these graphs are based appear in Appendix A.[2]. The
underlying data are the daily MAX and MIN measured in degrees Fahrenheit, obtained
from the U.S. National Ocean and Atmospheric Administration's Global Historical Climate
Network database (GHCN-daily).[3] Our sample period is from 01/01/1960 to 12/31/2017,
which covers the period of almost all recent climate change.

2.1   Distributions

The daily MAX and MIN are informative of both the central tendency and variability of
the daily continuous-time temperature record. In particular, the daily average temperature,
AVG=(MAX+MIN)/2, is a natural measure of central tendency, and the daily temperature
range, DTR=MAX-MIN, is a natural measure of volatility or variability. DTR is not only a
natural and intuitive estimator of daily volatility, but it is also highly efficient statistically.
The "daily range" has a long and distinguished tradition of use in econometrics due to its
good properties in estimating underlying quadratic variation from discretely-sampled data
(Alizadeh et al., 2002). AVG has been studied and modeled extensively (Raftery et al.,

---

[2]EViews code is available at `https://www.sas.upenn.edu/~fdiebold/papers/paper122/DTRcode.txt`
[3]The data are available at `https://www.ncdc.noaa.gov/ghcn-daily-description`. For details, see
Menne et al. (2012) and Jaffres (2019).

Figure 2: Data and Estimated Trends, AVG and DTR, Philadelphia
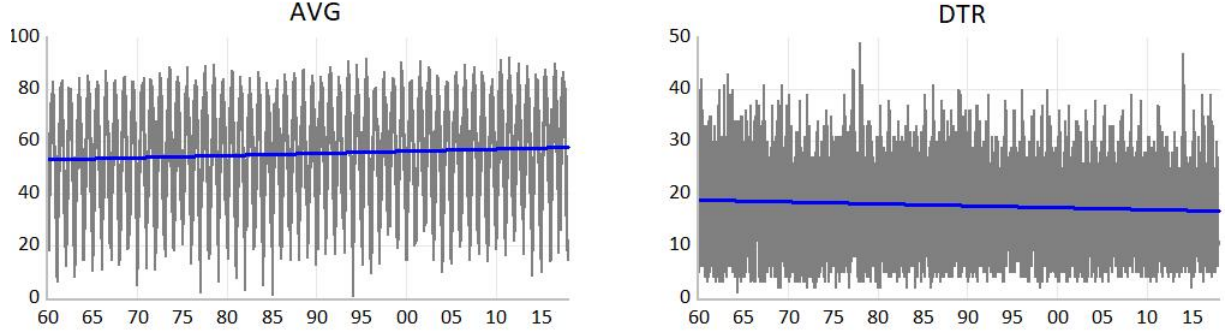
Notes to figure: We show time series of daily AVG and DTR (gray) together with estimated linear trends (blue), 1960-2017. The vertical axes are scaled differently in the two panels, and they are in degrees Fahrenheit.

2017), and DTR much less so.

In Figure 1, we show kernel estimates of the unconditional densities of AVG and DTR. The bimodal shape of the AVG density reflects the strong seasonality in AVG. The "winter mode" is around 40°F, and the "summer mode" is around 75°F. The AVG density contrasts sharply with the unimodal approximately-symmetric density of DTR, which is centered around 19°F and much less dispersed.

2.2   Trend

In Figure 2, we display time series plots of the entire data sample of AVG and DTR with fitted linear trends superimposed. The regression is

$$Y \rightarrow c, TIME, \tag{1}$$

where Y is AVG or DTR, c is a constant, and $TIME$ is a time trend (that is, $TIME_t = t$ and $t = 1, ..., T$). Here and throughout, we use Newey and West (1987) heteroskedasticity and autocorrelation consistent (HAC) standard errors to assess statistical significance.

The AVG trend slopes upward and is statistically significant, which is consistent with the overall global warming during this period. The steepness of this trend is surprising, as the AVG trend grows by nearly five degrees Fahrenheit over the course of the 57-year 1960-2017

sample. This increment is a bit more than twice as much as the average global increase over the same period (Rudebusch, 2019). The faster upward trend in the Philadelphia airport average temperature likely reflects two key factors: (1) average temperatures in growing cities tend to rise more quickly due to an increasing urban heat island effect and (2) average land temperatures generally grow more quickly than the global average, which includes ocean areas that are slow to warm.

As for Philadelphia temperature variability, DTR also has a significant trend, and it slopes *downward*, dropping by more than two degrees over the course of the sample – a diurnal asymmetry. The downward DTR trend arises from different trends in the underlying MAX and MIN. Both trend upward, but MIN is on a steeper incline as evening temperatures warm more quickly. Hence, the spread between MAX and MIN tends to shrink, and DTR decreases over time. As noted by Dai et al. (1999), Davy et al. (2017), and Vinnarasi et al. (2017), such a downward trend is not found at all locations; however, the relatively muted upward trend in MAX can generally be ascribed to increased cloud cover, soil moisture, and precipitation, which lead to decreased surface solar radiation and increased daytime surface evaporative cooling.

The overall picture, then, involves not only an upward trend in AVG, but also a gradual tightening of daily fluctuations around that trend. Warming is not only happening, but progressively less volatility as well. As a result, the increases in heat are becoming harder to avoid at night, with potentially adverse consequences that likely fall disproportionately on the poor and vulnerable.

2.3   Fixed Seasonality

In Figure 3, we show the actual and fitted values from regressions of de-trended AVG and DTR on 12 monthly seasonal dummies,

$$\widetilde{Y} \ \rightarrow \ D_1, ..., D_{12}, \tag{2}$$

where $\widetilde{Y}$ is de-trended AVG or DTR – the residuals from regression (1) – and $D_{it} = 1$ if day t is in month i, and 0 otherwise.[4] This model is effectively an intercept regression for deviations from trend, allowing for a different intercept each month.

As shown in the top panel of Figure 3, AVG displays pronounced seasonality. The

---

[4]There is of course no need for an intercept, which would be completely redundant and hence cause perfect multicollinearity.

Figure 3: De-Trended Data and Estimated Fixed Seasonals, AVG and DTR, Philadelphia
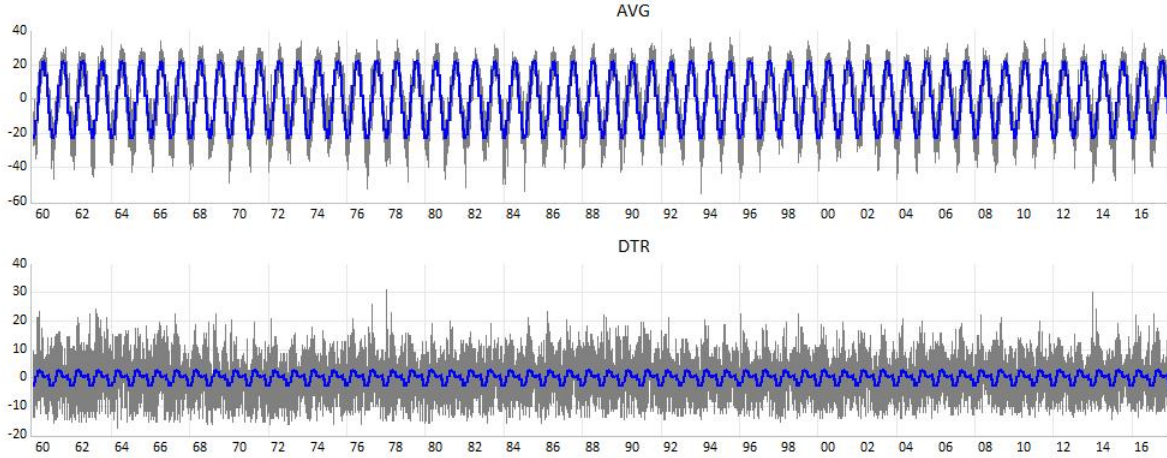
Notes to figure: We show time series of daily linearly de-trended AVG and DTR (gray) together with estimated fixed seasonals (blue) from regressions of daily linearly de-trended data on 12 monthly seasonal dummies, 1960-2017. The vertical and horizontal axes are scaled identically in the top and bottom panels. The vertical axes are in degrees Fahrenheit.

seasonality is highly significant and is responsible for a large amount AVG variation. The R^2 of the seasonal AVG regression (2) is .81. As with the upward trend in AVG, strong seasonality in deviations of AVG from its trend is hardly surprising – it's cold in the winter and hot in the summer.

There is also significant seasonality in DTR, as shown in the bottom panel of Figure 3. The DTR seasonality was hard to detect visually in the time series plot of Figure 2, because it is buried in much more noise than that of AVG. The R^2 of the seasonal DTR regression (2) is only .07.

In Figure 4, we show the estimated monthly seasonal factors for AVG (left panel) and DTR (right panel). They are simply the 12 estimated coefficients on the 12 monthly dummies in the seasonal regression (2). The seasonal pattern for AVG is as expected – smooth and unimodal, high in the summer and low in the winter, achieving its maximum in July and its minimum in January. In contrast, the seasonal pattern for DTR is clearly bi-modal, with one mode in April-May and one in October. DTR's two annual peaks (spring and fall) and two annual troughs (winter and summer) contrast sharply with AVG's single annual peak (summer) and single annual trough (winter). This "twin-peaks" or "M-shaped" DTR

6

Figure 4: Estimated Fixed Twelve-Month Seasonal Patterns, AVG and DTR, Philadelphia
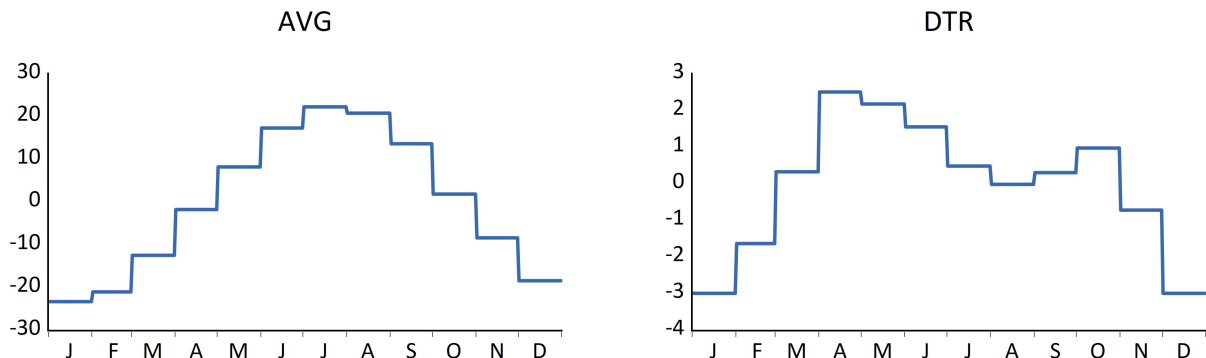
Notes to figure: We show estimated fixed twelve-month seasonal patterns for AVG and DTR, based on regressions of daily linearly de-trended data on 12 monthly seasonal dummies, 1960-2017. The vertical axes are scaled differently in the left and right panels, and they are in degrees Fahrenheit.

pattern is common across many U.S. cites. Moreover, as we shall show, in many locations, the DTR seasonal pattern has evolved noticeably over time with climate change.

2.4 Evolving Seasonality

The AVG and DTR trends documented thus far are trends in *level*. More subtle are trends in *seasonality* – that is, trends in the tent-shaped AVG seasonal pattern and the M-shaped DTR seasonal pattern. In that case, the seasonal patterns shown in Figure 4, estimated over the full sample 1960-2017, would be the sample averages that would not capture the evolution of the distribution over time.

We now explore the possibility of evolving seasonality by allowing for trends in the seasonal factors. Mechanically, this involves regressing de-trended AVG or DTR not only on 12 monthly dummies, but also those same 12 dummies interacted with time,

$$\widetilde{Y} \ \rightarrow \ D_1, ..., D_{12}, \ \ D_1{\cdot}TIME, ..., D_{12}{\cdot}TIME, \tag{3}$$

where $\widetilde{Y}$ is de-trended AVG or DTR, $D_{it} = 1$ if day t is in month i and 0 otherwise, and $TIME_t = t$. Regression (3) can capture linearly-trending seasonal deviations from a linear trend. Effectively, it allows for a different intercept each month, with those intercepts themselves potentially trending at different rates. In the special case where all interaction

7

Figure 5: Estimated Evolving Twelve-Month Seasonal Patterns, DTR and AVG, Philadelphia, 1960 vs. 2017
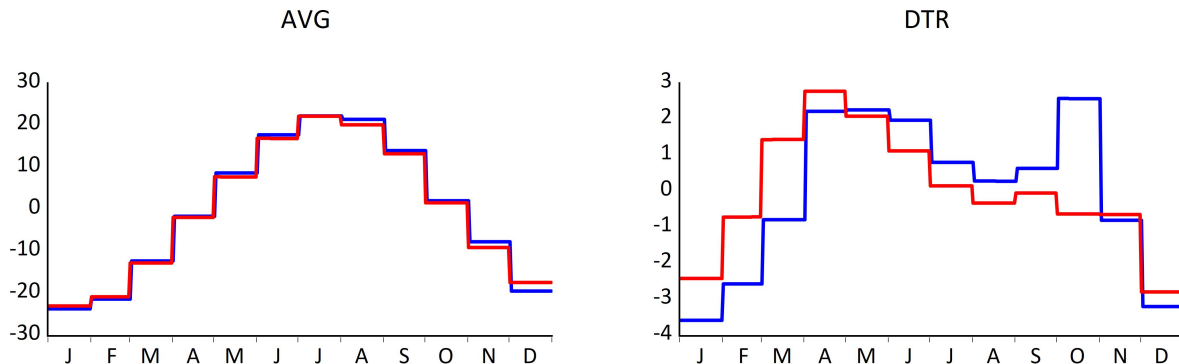
Notes to figure: We show the estimated twelve-month seasonal patterns of AVG and DTR, based on regressions of daily linearly de-trended data on 12 monthly seasonal dummies, and those same dummies interacted with time, 1960-2017. 1960 is blue, and 2017 is red. The vertical axes are scaled differently in the left and right panels, and they are in degrees Fahrenheit.

coefficients are zero, it collapses to fixed seasonal deviations from linear trend, as explored in section 2.3.

For AVG, there are no gains from estimating the more flexible seasonal specification (3). The interaction terms are universally insignificantly different from zero, clearly indicating no change over time in the AVG seasonal pattern. In the left panel of Figure 5, we show the estimated seasonal factors for AVG for the first year (1960) and last year (2017) of our sample. This range provides the maximum contrast, but the two seasonal patterns are nevertheless essentially identical.

The results for DTR, however, are very different. Unlike the AVG seasonal, which does not evolve, the DTR seasonal changes significantly over time. The January-through-March DTR interaction coefficients are significantly positive, indicating that the winter DTR low is increasing. In addition, all May-through-October interaction coefficients are negative, and the October coefficient is large and highly significantly negative. This corresponds to progressively lower DTR highs in Octobers, so that the fall DTR peak is gradually vanishing. Both effects (higher winter DTR lows, and lower fall DTR highs) are visually apparent in the right panel of Figure 5, in which we contrast the estimated DTR M-shaped seasonal pattern in the first year (1960) and last year (2017) of our sample.

Figure 6: Fifteen Cities
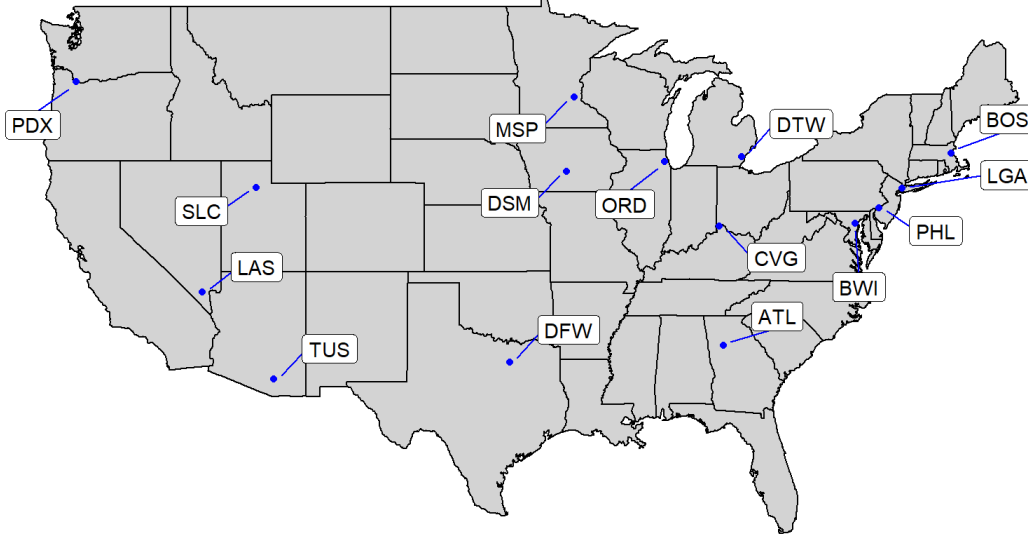
Note to figure: We show the fifteen cities for which we study AVG and DTR, by airport code.

3 Fifteen Cities

We now expand our analysis to include data from the airports of the fifteen U.S. cities shown in Figure 6. As with the Philadelphia case study in section 2, we obtain the underlying daily MAX and MIN data, from which we construct daily AVG and DTR, from the U.S. National Ocean and Atmospheric Administration's GHCN-daily, `https://www.ncdc.noaa.gov/ghcn-daily-description`. Our sample period is 01/01/1960-12/31/2017.[5]

We choose these city weather reporting stations because all of them have had temperature derivatives traded on the Chicago Merchantile Exchange (CME). Consideration of such CME cities is of interest for several reasons. First, these locations cover a diverse set of climates, so they can provide a check of the robustness of our Philadelphia results. Second, they are urban locations that represent large numbers of people and a sizable share of economic activity – one reason that their CME contracts are traded. Finally, the valuations of weather derivatives traded in financial markets depend on the evolution of the stochastic structure of

---

[5]There were a (very) few missing observations, in which case we interpolated using an average of the immediately previous and subsequent days' values, rounded to the nearest integer. The missing observations are: BWI max: 1/7/04, min: 1/6/04, DSM max: 9/15/96, min: 9/15/96, and TUS max: 5/10/10, 8/18/17, 8/19/17, min: 5/11/10, 8/18/17, 8/19/17.

temperature dynamics, which is precisely the focus of our modeling efforts and so naturally paired with the CME cities.

The full set of historically-traded cities includes: Atlanta, ATL; Boston, BOS; Baltimore Washington, BWI; Chicago, ORD; Cincinnati, CVG; Dallas Fort Worth, DFW; Des Moines, DSM; Detroit, DTW; Houston, IAH; Kansas City, MCI; Las Vegas, LAS; Minneapolis St Paul, MSP; New York, LGA; Portland, PDX; Philadelphia, PHL; Sacramento, SAC; Salt Lake City, SLC, and Tuscon, TUS.[6] We exclude Houston, Kansas City, and Sacramento, however, due to large amounts of missing data, leaving fifteen cities. Presently eight cities are traded (Atlanta, Chicago, Cincinnati, Dallas, Las Vegas, Minneapolis, New York, and Sacramento), and all but Sacramento are in our fifteen.[7]

In addition to expanding our analysis to include more cities, we also employ a more sophisticated modeling approach that *jointly* captures trend, seasonality, and serial correlation, and we implement it for both conditional-mean and conditional-variance dynamics. Our approach builds on Campbell and Diebold (2005), but with several important differences. We study the variability as well as the central tendency of temperature, explore time-varying seasonality, and consider more cities and a longer data sample.

3.1   Conditional Mean Dynamics

We view the sequential approach employed in section 2 – fitting a trend and then characterizing seasonality in the de-trended data – as intuitive and transparent. We now consolidate and extend various aspects of that approach, to arrive at a simple yet powerful joint model. Regarding consolidation, we move from a multi-step sequential conditional mean modeling approach to a single-step joint approach with a single conditional mean estimation. Regarding extension, we now include an autoregressive lag in the model. The single autoregressive lag facilitates simple assessment of the strength of serial correlation in the deviations from the trend/seasonal, and it also provides potentially valuable pre-whitening for HAC covariance matrix estimation, as emphasized in Andrews and Monahan (1992).

We proceed by regressing AVG or DTR on an intercept and 11 monthly seasonal dummies to capture seasonal intercept variation (we drop July, so the included constant captures July and all estimated seasonal effects are relative to July), a linear trend and 11 seasonal dummies interacted with it to capture seasonal trend slope variation (we drop the July interaction),

---

[6]See `ftp://ftp.cmegroup.com/weather/usa/temperature/historical/daily`.
[7]See `https://www.cmegroup.com/trading/weather/temperature-based-indexes.html`.

Table 1: AVG, Conditional Mean Dynamics, Fifteen Cities

(1) station	(2) $\Delta trend$	(3) $p(nt)$	(4) $p(ns)$	(5) $p(nts)$	(6) ρ	(7) R^2
ATL	4.36*	0.00	0.00	0.00	0.76*	0.90
BOS	2.06*	0.00	0.00	0.73	0.67*	0.89
BWI	2.25*	0.00	0.00	0.80	0.71*	0.90
CVG	2.53	0.04	0.00	0.94	0.74*	0.89
DFW	3.44*	0.00	0.00	0.55	0.72*	0.89
DSM	3.93*	0.00	0.00	0.17	0.76*	0.91
DTW	4.09*	0.00	0.00	0.99	0.74*	0.91
LAS	6.05*	0.00	0.00	0.41	0.82*	0.96
LGA	4.03*	0.00	0.00	0.97	0.71*	0.91
MSP	4.72*	0.00	0.00	0.18	0.77*	0.93
ORD	2.86*	0.00	0.00	0.78	0.74*	0.90
PDX	2.55*	0.00	0.00	0.26	0.76*	0.90
PHL	4.78*	0.00	0.00	0.95	0.72*	0.91
SLC	3.92*	0.00	0.00	0.67	0.77*	0.93
TUS	4.89*	0.00	0.00	0.33	0.79*	0.93
Median	3.93	0.00	0.00	0.67	0.74	0.91

Notes to table: All results are based on daily data, 1960-2017. Column 1 reports measurement station by airport code. Column 2 reports the estimated trend movement over the entire 57-year sample in degrees Fahrenheit, using a simple regression on linear trend. The remaining columns report results from the conditional-mean regression (4). $p(nt)$ is the robust p-value for a Wald test of no trend (all coefficients on TIME and $D \cdot TIME$ interactions are 0), $p(ns)$ is the robust p-value for a Wald test of no seasonality (all coefficients on D's and $D \cdot TIME$ interactions are 0), and $p(nts)$ is the robust p-value for Wald a test of no trend in seasonality (all coefficients on $D \cdot TIME$ interactions are 0). ρ is the estimated autoregressive coefficient, and R^2 is the coefficient of determination. Asterisks denote significance at the one percent level. See text for details.

Table 2: DTR, Conditional Mean Dynamics, Fifteen Cities

(1) station	(2) $\Delta trend$	(3) $p(nt)$	(4) $p(ns)$	(5) $p(nts)$	(6) ρ	(7) R^2
ATL	-1.65*	0.00	0.00	0.14	0.38*	0.18
BOS	-0.48*	0.00	0.00	0.00	0.25*	0.10
BWI	-0.43	0.34	0.00	0.50	0.38*	0.19
CVG	-1.31*	0.00	0.00	0.04	0.32*	0.17
DFW	-1.31*	0.00	0.00	0.64	0.40*	0.17
DSM	-0.51*	0.00	0.00	0.03	0.32*	0.15
DTW	-2.88*	0.00	0.00	0.00	0.33*	0.27
LAS	-7.02*	0.00	0.00	0.13	0.46*	0.37
LGA	0.03*	0.00	0.00	0.00	0.23*	0.14
MSP	-3.07*	0.00	0.00	0.00	0.31*	0.18
ORD	-2.03*	0.00	0.00	0.00	0.30*	0.20
PDX	-1.68*	0.00	0.00	0.63	0.50*	0.45
PHL	-2.13*	0.00	0.00	0.00	0.34*	0.19
SLC	-4.21*	0.00	0.00	0.00	0.44*	0.47
TUS	0.48	0.05	0.00	0.03	0.51*	0.35
Median	-1.65	0.00	0.00	0.03	0.34	0.19

Notes to table: See Table 1.

and a first-order autoregressive lag:[8]

$$Y \ \rightarrow \ c, TIME, Y(-1), D_1, ..., D_6, D_8, ..., D_{12}, D_1 \cdot TIME, ..., D_6 \cdot TIME, D_8 \cdot TIME, ..., D_{12} \cdot TIME, \quad (4)$$

where Y is AVG or DTR, $TIME_t = t$, $Y(-1)$ denotes a 1-day lag, and $D_{it} = 1$ if day t is in month i and 0 otherwise. The joint model (4) allows for different intercepts each month, with the different intercepts potentially trending linearly at different rates, and for serially correlated deviations from the trend/seasonal.[9] We summarize the estimation results in Tables 1 and 2, in which we show the weather station identifier (airport code) in column 1, and various aspects of the estimation results in subsequent columns.[10]

---

[8]We continue to use HAC standard errors despite the inclusion of a first-order autoregressive lag, both because we view the autoregressive lag as a simple pre-whitening strategy rather than a definitive model of serial correlation, and to maintain robustness to heteroskedasticity in temperature shocks.

[9]We have explored – and generally confirmed – the robustness of our results by comparing them to those obtained from a more flexible model with quadratic terms as well as assessing the structural stability of regressions.

[10]Detailed regression results for all cities are in the online Appendix B (https://www.sas.upenn.edu/~fdiebold/papers/paper122/OnlineAppendix.pdf.txt, and underlying EViews code is at https://www.sas.upenn.edu/~fdiebold/papers/paper122/DTRcode.txt.

3.1.1 Trend

As shown in column 2 of Table 1, the estimated AVG trend movements over the full sample are large and positive in each city. They are also all highly statistically significant (column 3), with a median p-value of 0.00 for Wald tests of the null hypothesis of no trend. These p-values are denoted $p(nt)$, where "nt" stands for "no trend", which corresponds to zero coefficients on TIME and all TIME interactions in regression (4) (in which case it collapses to seasonal intercepts with serial correlation). The median estimated trend movement is 3.38°F, greater than the consensus estimate of the increase in the mean global temperature over the same period, as U.S. airports have warmed more quickly than the global average.

Similarly, in column 2 of Table 2, we report the estimated full-sample trend movements for DTR. All but one are negative, and most are significant at the one percent level. The median estimated trend movement is -1.45°F, with a median p-value, $p(nt)$, of 0.00 for the no-trend null hypothesis (column 3). Interestingly, LAS, which has the largest *upward* AVG trend, also has the largest *downward* DTR trend.

3.1.2 Seasonality

In column 4 of Tables 1 and 2, we report p-values for Wald tests of the hypothesis of no AVG and DTR seasonality, respectively. These p-values are denoted $p(ns)$, where "ns" stands for "no seasonality", which corresponds to zero coefficients on all included seasonal dummies and dummy interactions in regression (4) (in which case it collapses to linear trend with serial correlation). There is of course strong evidence of seasonality in AVG with all $p(ns)$'s equal to 0.00. Less well known is the similarly strong seasonality in DTR with all $p(ns)$'s again equal to 0.00.

In column 5 of Tables 1 and 2, we report p-values for Wald tests of the hypothesis of no evolving (i.e., trending) AVG and DTR seasonality, respectively. These p-values are denoted $p(nts)$, where "nts" stands for "no trending seasonality", which corresponds to zero coefficients on all seasonal dummy interactions in regression (4) (in which case it collapses to linear trend and fixed seasonal dummies with serial correlation). The results are striking. There is no evidence for evolving seasonality in AVG; the median AVG $p(nts)$ is 0.67. In contrast, there is strong evidence of evolving seasonality in DTR; the median DTR $p(nts)$ is 0.03.

3.1.3 Serial Correlation

Estimated AVG and DTR serial correlation coefficients appear in column 6 of Tables 1 and 2, respectively. All are positive and significant at the one percent level. Their magnitudes, however, are very different. All those for AVG are around 0.75, whereas all those for DTR are around 0.35.

It is interesting to note that, although the signal in both AVG and DTR is clearly driven by trend, seasonal, and cyclical components, the AVG signal is buried in much less noise. As shown in column 7 of Tables 1 and 2, respectively, all AVG regression R^2 values are around 0.9, whereas all those for DTR are around 0.2.

3.2 Conditional Variance Dynamics

To allow for residual heteroskedasticity, we proceed exactly as in the conditional mean regression, whether for AVG or DTR, except that the left-hand-side variable is now a *squared residual* from the conditional mean regression:

$$e^2 \rightarrow c, TIME, e^2(-1), D_1, ..., D_6, D_8, ..., D_{12}, D_1 \cdot TIME, ..., D_6 \cdot TIME, D_8 \cdot TIME, ..., D_{12} \cdot TIME. \quad (5)$$

The key point is that residual signs don't matter in the conditional-variance regression (5), because the residuals are *squared*. Instead the regression explains the squared variation in the residuals, which is their *volatility*, or more precisely (in conditional expectation) their conditional variance. The conditional-variance regression results appear in Tables 3 and 4, which are in precisely the same format as our earlier conditional-mean Tables 1 and 2.

Interestingly, AVG and DTR conditional variance e^2 dynamics display the same component structure as did the conditional mean dynamics, although the patterns of trend and seasonality differ. The trend patterns are similarly downward for both AVG and DTR. The seasonal patterns are similarly high in the winter for both AVG and DTR. The conditional variance trend and seasonal effects tend to be significant, but the conditional variance regressions are noisy, with R^2's around 0.05.

3.3 Shock Distributions

Armed with estimates of residual conditional standard deviations (the square roots of the fitted values from regression (5)), we can examine the densities of standardized residuals, that is the densities of the ultimate underlying AVG and DTR shocks. We show their skewness and kurtosis in Table 5. For each station, skewness is approximately 0 and kurtosis

Table 3: AVG, Conditional Variance Dynamics, Fifteen Cities

(1) station	(2) $\Delta trend$	(3) $p(nt)$	(4) $p(ns)$	(5) $p(nts)$	(6) ρ	(7) R^2
ATL	-0.29	0.23	0.00	0.34	0.07*	0.11
BOS	-0.01	0.02	0.00	0.02	0.07*	0.04
BWI	-0.03	0.44	0.00	0.54	0.05*	0.06
CVG	-0.43*	0.00	0.00	0.52	0.04*	0.10
DFW	-0.11	0.82	0.00	0.77	0.09*	0.11
DSM	-0.34*	0.00	0.00	0.25	0.05	0.08
DTW	-0.53*	0.00	0.00	0.07	0.05*	0.05
LAS	-0.61	0.46	0.00	0.39	0.09*	0.03
LGA	-0.04	0.36	0.00	0.52	0.06*	0.05
MSP	-0.79*	0.00	0.00	0.00	0.04*	0.08
ORD	-0.79*	0.00	0.00	0.40	0.04*	0.05
PDX	-0.03	0.38	0.00	0.30	0.10*	0.02
PHL	-0.25*	0.00	0.00	0.29	0.05*	0.06
SLC	-0.14	0.05	0.00	0.04	0.08*	0.02
TUS	0.02	0.03	0.00	0.03	0.03*	0.04
Median	-0.25	0.03	0.00	0.30	0.05	0.05

Notes to table: All results are based on daily data, 1960-2017. Column 1 reports measurement station by airport code. Column 2 reports the estimated trend movement over the entire 57-year sample in degrees Fahrenheit, using a regression of absolute residuals from conditional-mean regression (4) on linear trend. (We use absolute rather than squared residuals for the column 2 regression to keep the units in degress Fahrenheit.) The remaining columns report results from the conditional-variance regression (5). $p(nt)$ is the robust p-value for a Wald test of no trend (all coefficients on TIME and $D{\cdot}TIME$ interactions are 0), $p(ns)$ is the robust p-value for a Wald test of no seasonality (all coefficients on D's and $D{\cdot}TIME$ interactions are 0), and $p(nts)$ is the robust p-value for Wald a test of no trend in seasonality (all coefficients on $D{\cdot}TIME$ interactions are 0). ρ is the estimated autoregressive coefficient, and R^2 is the coefficient of determination. Asterisks denote significance at the one percent level. See text for details.

Table 4: DTR, Conditional Variance Dynamics, Fifteen Cities

(1) station	(2) $\Delta trend$	(3) $p(nt)$	(4) $p(ns)$	(5) $p(nts)$	(6) ρ	(7) R^2
ATL	-0.86*	0.00	0.00	0.00	0.01	0.10
BOS	-0.28	0.13	0.00	0.65	0.07*	0.03
BWI	-0.32	0.31	0.00	0.90	0.04*	0.04
CVG	-0.64*	0.00	0.00	0.72	0.03*	0.05
DFW	-0.44	0.12	0.00	0.91	0.03*	0.11
DSM	-0.50*	0.01	0.00	0.87	0.01	0.06
DTW	-1.14*	0.00	0.00	0.00	0.05*	0.03
LAS	-1.23*	0.00	0.00	0.00	0.04*	0.04
LGA	-0.47*	0.00	0.00	0.14	0.06*	0.03
MSP	-1.44*	0.00	0.00	0.26	0.04*	0.03
ORD	-1.05*	0.00	0.00	0.02	0.04*	0.03
PDX	-0.79*	0.00	0.00	0.01	0.00	0.05
PHL	-0.89*	0.00	0.00	0.02	0.07*	0.05
SLC	-0.77*	0.00	0.00	0.02	0.05*	0.02
TUS	0.21	0.15	0.00	0.63	0.01	0.04
Median	-0.77	0.00	0.00	0.14	0.04	0.04

Notes to table: See Table 3.

is approximately 3, corresponding to conditional normality. Indeed for DTR the median skewness and kurtosis are 0.00 and 3.00, respectively.

4 Concluding Remarks

Climate change is one of the most consequential and pressing issues of our time. We have focused on DTR as an important summary statistic for characterizing climate change. We have provided new stochastic time series representations of DTR that can capture in particular its evolving seasonality. Throughout we have also provided parallel contrasting results for AVG. Indeed the results in Tables 1-5 provide a detailed summary of both DTR and AVG stochastic structure.

Our results may prove useful for assessing and improving structural climate models. In previous research, Braganza et al. (2010), Zhou et al. (2010), Lewis and Karoly (2013), and Rader et al. (2018) show that DTR is a useful metric to help assess the accuracy and degree of fit of global climate models. They generally found that these models persistently

Table 5: Skewness and Kurtosis, Standardized Residuals, Fifteen Cities

| (1) | (2) | (3) | (4) | (5) |
| | AVG | | DTR | |
station	*skew*	*kurt*	*skew*	*kurt*
ATL	-0.68	3.74	-0.32	3.19
BOS	0.06	2.96	0.43	3.23
BWI	-0.13	3.15	-0.09	2.92
CVG	-0.31	3.23	0	2.86
DFW	-0.64	4.10	-0.08	3.25
DSM	-0.18	3.17	0.13	2.96
DTW	-0.07	3.14	0.09	2.98
LAS	-0.76	4.51	-0.44	3.07
LGA	-0.14	3.02	0.43	3.55
MSP	-0.12	3.17	0.22	3.00
ORD	-0.13	3.24	0.16	2.90
PDX	0.04	3.14	0.11	2.80
PHL	-0.20	3.09	-0.06	3.02
SLC	-0.50	3.77	-0.28	2.98
TUS	-0.69	4.16	-0.53	3.37
Median	-0.18	3.17	0.00	3.00

Notes to table: We show sample skewness and kurtosis of residuals from the conditional-mean regression (4) divided by square roots of fitted values from the conditional-variance regression (5). See text for details.

underestimated the trend in DTR, which was likely related to deficiencies in modeling water vapor and cloud cover processes. Our new results on the evolving seasonality of DTR may provide an additional, more refined, benchmark for such evaluations.

Our results may also prove useful for assessing financial market efficiency, that is, for assessing whether the temperature forecasts embedded in financial asset prices accurately reflect temperature's underlying dynamics. Schlenker and Taylor (2019) address this issue focusing on AVG, and it may be of interest to extend their analysis to incorporate our more complete model of AVG dynamics, or to consider a multivariate modeling of AVG and DTR extending the univariate approach undertaken in this paper.

References

Alexander, L. and S. Perkins (2013), "Debate Heating up Over Changes in Climate Variability," *Environmental Research Letters*, 8, 041001.

Alizadeh, S., M. Brandt, and F.X. Diebold (2002), "Range-Based Estimation of Stochastic Volatility Models," *Journal of Finance*, 57, 1047–1092.

Andrews, D.W.K. and J.C. Monahan (1992), "An Improved Heteroskedasticity and Autocorrelation Consistent Covariance Matrix Estimator," *Econometrica*, 60, 953–966.

Braganza, K., D.J. Karoly, and J.M Arblaster (2010), "Diurnal Temperature Range as an Index of Global Climate Change During the Twentieth Century," *Geophysical Research Letters*, 31, l13217, doi:10.1029/2004GL019998.

Campbell, S.D. and F.X. Diebold (2005), "Weather Forecasting for Weather Derivatives," *Journal of the American Statistical Association*, 100, 6–16.

Dai, A., K.E. Trenberth, and T.R. Karl (1999), "Effects of Clouds, Soil Moisture, Precipitation, and Water Vapor on Diurnal Temperature Range," *Journal of Climate*, 12, 2451–2473.

Davy, R., I. Esau, A. Chernokulsky, S. Outten, and S. Zilitinkevich (2017), "Diurnal Asymmetry to the Observed Global Warming," *International Journal of Climatology*, 37, 79–93.

Durre, I. and J.M. Wallace (2001), "The Warm Season Dip in Diurnal Temperature Range over the Eastern United States," *Journal of Climate*, 14, 354–360.

Hsiang, S. and R.E. Kopp (2018), "An Economist's Guide to Climate Change Science," *Journal of Economic Perspectives*, 32, 3–32.

Jackson, L.S. and P.M. Forster (2010), "An Empirical Study of Geographic and Seasonal Variations in Diurnal Temperature Range," *Journal of Climate*, 23, 3205–3221.

Jaffres, J.B.D. (2019), "GHCN-Daily: A Treasure Trove of Climate Data Awaiting Discovery," *Computers and Geosciences*, 122, 35–44.

Lewis, S.C. and D.J. Karoly (2013), "Evaluation of Historical Diurnal Temperature Range Trends in CMIP5 Models," *Journal of Climate*, 26, 9077–9089.

Masson-Delmotte, V., P. Zhai, H.O. Pörtner, D. Roberts, J. Skea, P.R. Shukla, A. Pirani, C. Moufouma-Okia, C. Péan, R. Pidcock, S. Connors, J.B.R. Matthews, Y. Chen, X. Zhou, M.I. Gomis, E. Lonnoy, T. Maycock, M. Tignor, and T. Waterfield (eds.) (2018), *IPCC, 2018: Global Warming of 1.5 Degrees C. An IPCC Special Report on the Impacts of Global Warming of 1.5 Degrees C Above Pre-Industrial Levels and Related Global Greenhouse Gas Emission Pathways, in the Context of Strengthening the Global Response to the Threat of Climate Change, Sustainable Development, and Efforts to Eradicate Poverty*, `http://www.ipcc.ch/report/sr15/`.

Menne, M.J., I. Durre, R.S. Vose, B.E. Gleason, and T.G. Houston (2012), "An Overview of the Global Historical Climatology Network Daily Database," *Journal of Atmospheric and Oceanic Technology*, 29, 897–910.

Newey, W.K. and K.D. West (1987), "A Simple, Positive Semi-definite, Heteroskedasticity and Autocorrelation Consistent Covariance Matrix," *Econometrica*, 55, 703–708.

Qu, M., J. Wan, and X. Hao (2014), "Analysis of Diurnal Air Temperature Range Change in the Continental United States," *Weather and Climate Extremes*, 4, 86–95.

Rader, J., K.B. Karnauskas, and J.Y. Luo (2018), "Diurnal Temperature Variability: an Observations-Climate Model Intercomparison," Unpublished Manuscript.

Raftery, A. E., A. Zimmer, D. M. W. Frierson, R. Startz, and P. Liu (2017), "Less Than 2°C Warming by 2100 Unlikely," *Nature Climate Change*, 7, 637–641.

Reidmiller, D.R., C.W. Avery, D.R. Easterling, K.E. Kunkel, K.L.M. Lewis, T.K. Maycock, and B.C. Stewart (eds.) (2018), *USGCRP, 2018: Impacts, Risks, and Adaptation in the United States: Fourth National Climate Assessment, Volume II*, U.S. Global Change Research Program, Washington, DC, USA. doi: 10.7930/NCA4.2018, `https://nca2018.globalchange.gov/chapter/front-matter-guide`.

Robinson, J. (2006), *The Oxford Companion to Wine*, Third Edition, Oxford University Press.

Rudebusch, G.D. (2019), "Climate Change and the Federal Reserve," *FRBSF Economic Letter*.

Ruschy, D.L., D.G. Baker, and R.H. Skaggs (1991), "Seasonal Variation in Daily Temperature Ranges," *Journal of Climate*, 4, 1211–1216.

Sun, D. and R. Pinker (2014), "Factors Contributing to the Spatial Variability of Satellite Estimates of Diurnal Temperature Range in the United States," *IEEE Geoscience and Remote Sensing Letters*, 11, 1524–1528.

Vinnarasi, R., C.T. Dhanya, A. Chakravorty, and A. AghaKouchak (2017), "Unravelling Diurnal Asymmetry of Surface Temperature in Different Climate Zones," *Nature.com Scientific Reports, Volume 7, Article 7350, https://www.nature.com/articles/s41598-017-07627-5*.

Wigglesworth, D.S. (2019), "Crop Production and Climate Change: The Importance of Temperature Variability," Unpublished Thesis, University of Pennsylvania.

Zhou, L., R.E. Dickinson, A. Dai, and P. Dirmeyer (2010), "Detection and Attribution of Anthropogenic Forcing to Diurnal Temperature Range Changes from 1950 to 1999: Comparing Multi-model Simulations with Observations," *Climate Dynamics*, 35, 1289–1307.

Appendices

A Sequential and Joint Regression Results for Philadelphia

Figure A1: PHL Trend Regression, AVG

Dependent Variable: AVG_PHL
Method: Least Squares
Date: 07/09/19   Time: 13:46
Sample: 1/01/1960 12/31/2017
Included observations: 21185
HAC standard errors & covariance (Bartlett kernel, Newey-West fixed
    bandwidth = 14.0000)

Variable	Coefficient	Std. Error	t-Statistic	Prob.
C	53.02047	0.860367	61.62542	0.0000
TIME	0.000226	6.97E-05	3.237848	0.0012

R-squared	0.006068	Mean dependent var		55.41086
Adjusted R-squared	0.006021	S.D. dependent var		17.71674
S.E. of regression	17.66333	Akaike info criterion		8.580953
Sum squared resid	6608952.	Schwarz criterion		8.581704
Log likelihood	-90891.74	Hannan-Quinn criter.		8.581198
F-statistic	129.3170	Durbin-Watson stat		0.107062
Prob(F-statistic)	0.000000	Wald F-statistic		10.48366
Prob(Wald F-statistic)	0.001206			

Figure A2: PHL Trend Regression, DTR

Dependent Variable: DTR_PHL
Method: Least Squares
Date: 07/09/19   Time: 13:46
Sample: 1/01/1960 12/31/2017
Included observations: 21185
HAC standard errors & covariance (Bartlett kernel, Newey-West fixed
    bandwidth = 14.0000)

Variable	Coefficient	Std. Error	t-Statistic	Prob.
C	18.81577	0.171811	109.5146	0.0000
TIME	-0.000100	1.30E-05	-7.722985	0.0000

R-squared	0.009040	Mean dependent var	17.75171
Adjusted R-squared	0.008993	S.D. dependent var	6.461139
S.E. of regression	6.432020	Akaike info criterion	6.560549
Sum squared resid	876359.4	Schwarz criterion	6.561300
Log likelihood	-69490.61	Hannan-Quinn criter.	6.560794
F-statistic	193.2414	Durbin-Watson stat	1.220993
Prob(F-statistic)	0.000000	Wald F-statistic	59.64450
Prob(Wald F-statistic)	0.000000		

Figure A3: PHL Fixed Seasonal Regression, AVG

Dependent Variable: AVGDET_PHL
Method: Least Squares
Date: 07/09/19   Time: 13:46
Sample: 1/01/1960 12/31/2017
Included observations: 21185
HAC standard errors & covariance (Bartlett kernel, Newey-West fixed
    bandwidth = 14.0000)

Variable	Coefficient	Std. Error	t-Statistic	Prob.
D1	-23.30393	0.501435	-46.47449	0.0000
D2	-21.02927	0.482270	-43.60480	0.0000
D3	-12.45912	0.432459	-28.80997	0.0000
D4	-1.758657	0.380855	-4.617651	0.0000
D5	8.244852	0.350938	23.49374	0.0000
D6	17.32183	0.273401	63.35694	0.0000
D7	22.24082	0.218207	101.9252	0.0000
D8	20.79500	0.240577	86.43813	0.0000
D9	13.65797	0.337038	40.52355	0.0000
D10	1.849370	0.382281	4.837729	0.0000
D11	-8.365280	0.381983	-21.89963	0.0000
D12	-18.38047	0.453931	-40.49180	0.0000

R-squared	0.810549	Mean dependent var		-4.09E-16
Adjusted R-squared	0.810451	S.D. dependent var		17.66291
S.E. of regression	7.689949	Akaike info criterion		6.918272
Sum squared resid	1252072.	Schwarz criterion		6.922781
Log likelihood	-73269.79	Hannan-Quinn criter.		6.919743
Durbin-Watson stat	0.599680			

Notes: The regression is based on de-trended data. See text for details.

Figure A4: PHL Fixed Seasonal Regression, DTR

Dependent Variable: DTRDET_PHL
Method: Least Squares
Date: 07/09/19   Time: 13:46
Sample: 1/01/1960 12/31/2017
Included observations: 21185
HAC standard errors & covariance (Bartlett kernel, Newey-West fixed
     bandwidth = 14.0000)

Variable	Coefficient	Std. Error	t-Statistic	Prob.
D1	-2.991512	0.192368	-15.55099	0.0000
D2	-1.635110	0.231828	-7.053111	0.0000
D3	0.330347	0.259911	1.271004	0.2037
D4	2.503174	0.249080	10.04967	0.0000
D5	2.176853	0.224701	9.687776	0.0000
D6	1.552979	0.203088	7.646812	0.0000
D7	0.481646	0.176516	2.728617	0.0064
D8	-0.018021	0.161591	-0.111525	0.9112
D9	0.301301	0.198622	1.516957	0.1293
D10	0.977539	0.232409	4.206109	0.0000
D11	-0.717284	0.227973	-3.146351	0.0017
D12	-2.989081	0.189615	-15.76399	0.0000

R-squared	0.072506	Mean dependent var		-4.12E-16
Adjusted R-squared	0.072024	S.D. dependent var		6.431868
S.E. of regression	6.195915	Akaike info criterion		6.486224
Sum squared resid	812818.0	Schwarz criterion		6.490733
Log likelihood	-68693.33	Hannan-Quinn criter.		6.487695
Durbin-Watson stat	1.317632			

The regression is based on de-trended data. See text for details.

Figure A5: PHL Evolving Seasonal Regression, AVG

Dependent Variable: AVGDET_PHL
Method: Least Squares
Date: 07/09/19   Time: 13:46
Sample: 1/01/1960 12/31/2017
Included observations: 21185
HAC standard errors & covariance (Bartlett kernel, Newey-West fixed
   bandwidth = 14.0000)

Variable	Coefficient	Std. Error	t-Statistic	Prob.
D1	-23.64611	0.917908	-25.76088	0.0000
D2	-21.28787	0.914906	-23.26781	0.0000
D3	-12.23296	0.909260	-13.45376	0.0000
D4	-1.611997	0.788622	-2.044069	0.0410
D5	8.723673	0.694282	12.56503	0.0000
D6	17.74138	0.472155	37.57531	0.0000
D7	22.26663	0.396004	56.22834	0.0000
D8	21.46530	0.458948	46.77065	0.0000
D9	14.03163	0.725289	19.34628	0.0000
D10	2.092955	0.757859	2.761666	0.0058
D11	-7.665536	0.745067	-10.28839	0.0000
D12	-19.43088	0.896796	-21.66700	0.0000
D1*TIME	3.28E-05	7.58E-05	0.433257	0.6648
D2*TIME	2.47E-05	7.77E-05	0.318247	0.7503
D3*TIME	-2.16E-05	7.55E-05	-0.285878	0.7750
D4*TIME	-1.39E-05	6.18E-05	-0.225743	0.8214
D5*TIME	-4.54E-05	5.85E-05	-0.775604	0.4380
D6*TIME	-3.97E-05	4.00E-05	-0.992529	0.3210
D7*TIME	-2.43E-06	3.33E-05	-0.073084	0.9417
D8*TIME	-6.30E-05	3.76E-05	-1.673848	0.0942
D9*TIME	-3.50E-05	5.66E-05	-0.618641	0.5362
D10*TIME	-2.28E-05	6.08E-05	-0.374342	0.7082
D11*TIME	-6.52E-05	5.89E-05	-1.107436	0.2681
D12*TIME	9.76E-05	7.39E-05	1.320912	0.1865

R-squared	0.810805	Mean dependent var		-4.09E-16
Adjusted R-squared	0.810600	S.D. dependent var		17.66291
S.E. of regression	7.686924	Akaike info criterion		6.918051
Sum squared resid	1250378.	Schwarz criterion		6.927070
Log likelihood	-73255.45	Hannan-Quinn criter.		6.920993
Durbin-Watson stat	0.600496			

The regression is based on de-trended data. See text for details.

Figure A6: PHL Evolving Seasonal Regression, DTR

Dependent Variable: DTRDET_PHL
Method: Least Squares
Date: 07/09/19   Time: 13:46
Sample: 1/01/1960 12/31/2017
Included observations: 21185
HAC standard errors & covariance (Bartlett kernel, Newey-West fixed
    bandwidth = 14.0000)

Variable	Coefficient	Std. Error	t-Statistic	Prob.
D1	-3.573516	0.363325	-9.835601	0.0000
D2	-2.566527	0.448222	-5.726018	0.0000
D3	-0.789095	0.512080	-1.540962	0.1233
D4	2.218789	0.587126	3.779068	0.0002
D5	2.262578	0.441418	5.125705	0.0000
D6	1.987942	0.469947	4.230139	0.0000
D7	0.815669	0.401014	2.034017	0.0420
D8	0.294241	0.368614	0.798236	0.4247
D9	0.653211	0.466555	1.400072	0.1615
D10	2.621864	0.514676	5.094198	0.0000
D11	-0.799358	0.512271	-1.560420	0.1187
D12	-3.201644	0.420064	-7.621792	0.0000
D1*TIME	5.58E-05	3.13E-05	1.782775	0.0746
D2*TIME	8.91E-05	3.63E-05	2.453206	0.0142
D3*TIME	0.000107	3.62E-05	2.952952	0.0032
D4*TIME	2.70E-05	4.38E-05	0.617480	0.5369
D5*TIME	-8.13E-06	3.63E-05	-0.223813	0.8229
D6*TIME	-4.11E-05	3.32E-05	-1.237224	0.2160
D7*TIME	-3.15E-05	2.87E-05	-1.096358	0.2729
D8*TIME	-2.94E-05	2.72E-05	-1.078317	0.2809
D9*TIME	-3.30E-05	3.38E-05	-0.977116	0.3285
D10*TIME	-0.000154	3.76E-05	-4.090476	0.0000
D11*TIME	7.65E-06	3.80E-05	0.201179	0.8406
D12*TIME	1.98E-05	3.20E-05	0.617898	0.5366

R-squared	0.076429	Mean dependent var		-4.12E-16
Adjusted R-squared	0.075425	S.D. dependent var		6.431868
S.E. of regression	6.184552	Akaike info criterion		6.483118
Sum squared resid	809380.3	Schwarz criterion		6.492137
Log likelihood	-68648.43	Hannan-Quinn criter.		6.486061
Durbin-Watson stat	1.323264			

The regression is based on de-trended data. See text for details.

Figure A7: PHL Joint Conditional Mean Regression, AVG

Dependent Variable: AVG_PHL
Method: Least Squares
Date: 07/09/19   Time: 13:46
Sample (adjusted): 1/02/1960 12/31/2017
Included observations: 21184 after adjustments
HAC standard errors & covariance (Bartlett kernel, Newey-West fixed
    bandwidth = 14.0000)

Variable	Coefficient	Std. Error	t-Statistic	Prob.
C	21.20203	0.406242	52.19058	0.0000
TIME	6.68E-05	1.13E-05	5.890710	0.0000
D1	-13.00377	0.398518	-32.63032	0.0000
D2	-12.01654	0.399985	-30.04244	0.0000
D3	-9.477612	0.366252	-25.87730	0.0000
D4	-6.497795	0.316712	-20.51640	0.0000
D5	-3.590633	0.271226	-13.23852	0.0000
D6	-1.031422	0.224911	-4.585914	0.0000
D8	-0.281529	0.207881	-1.354279	0.1757
D9	-2.623407	0.270530	-9.697284	0.0000
D10	-5.887328	0.305137	-19.29406	0.0000
D11	-8.778265	0.325337	-26.98210	0.0000
D12	-11.86465	0.382181	-31.04459	0.0000
D1*TIME	7.51E-06	2.78E-05	0.270704	0.7866
D2*TIME	-5.17E-06	2.81E-05	-0.183774	0.8542
D3*TIME	-7.90E-06	2.69E-05	-0.293868	0.7689
D4*TIME	-6.22E-06	2.30E-05	-0.270271	0.7870
D5*TIME	-1.02E-05	2.24E-05	-0.455154	0.6490
D6*TIME	-2.41E-05	1.84E-05	-1.313423	0.1891
D8*TIME	-2.11E-05	1.68E-05	-1.254882	0.2095
D9*TIME	-1.35E-05	2.12E-05	-0.637214	0.5240
D10*TIME	-1.09E-05	2.32E-05	-0.470157	0.6382
D11*TIME	-1.16E-05	2.26E-05	-0.515052	0.6065
D12*TIME	1.82E-05	2.72E-05	0.668393	0.5039
AVG_PHL(-1)	0.718329	0.005105	140.7124	0.0000

R-squared	0.908718	Mean dependent var		55.41201
Adjusted R-squared	0.908614	S.D. dependent var		17.71637
S.E. of regression	5.355669	Akaike info criterion		6.195368
Sum squared resid	606907.6	Schwarz criterion		6.204763
Log likelihood	-65596.33	Hannan-Quinn criter.		6.198433
F-statistic	8776.620	Durbin-Watson stat		1.782252
Prob(F-statistic)	0.000000	Wald F-statistic		10401.85
Prob(Wald F-statistic)	0.000000			

27

Figure A8: PHL Joint Conditional Mean Regression, DTR

Dependent Variable: DTR_PHL
Method: Least Squares
Date: 07/09/19   Time: 13:46
Sample (adjusted): 1/02/1960 12/31/2017
Included observations: 21184 after adjustments
HAC standard errors & covariance (Bartlett kernel, Newey-West fixed
        bandwidth = 14.0000)

Variable	Coefficient	Std. Error	t-Statistic	Prob.
C	12.95271	0.302723	42.78740	0.0000
TIME	-8.61E-05	1.93E-05	-4.453194	0.0000
D1	-2.922818	0.369270	-7.915131	0.0000
D2	-2.173920	0.412045	-5.275928	0.0000
D3	-1.035858	0.441871	-2.344253	0.0191
D4	0.964259	0.481586	2.002259	0.0453
D5	0.990373	0.408136	2.426577	0.0153
D6	0.804887	0.403563	1.994453	0.0461
D8	-0.301248	0.360100	-0.836567	0.4028
D9	-0.093547	0.418681	-0.223433	0.8232
D10	1.209749	0.443337	2.728733	0.0064
D11	-1.082676	0.440556	-2.457523	0.0140
D12	-2.615967	0.393432	-6.649102	0.0000
D1*TIME	6.07E-05	2.91E-05	2.088017	0.0368
D2*TIME	7.69E-05	3.20E-05	2.406160	0.0161
D3*TIME	9.12E-05	3.15E-05	2.895508	0.0038
D4*TIME	3.91E-05	3.56E-05	1.097937	0.2722
D5*TIME	1.26E-05	3.16E-05	0.398334	0.6904
D6*TIME	-9.59E-06	2.88E-05	-0.333302	0.7389
D8*TIME	-1.36E-06	2.63E-05	-0.051623	0.9588
D9*TIME	-2.09E-06	3.02E-05	-0.069050	0.9450
D10*TIME	-8.02E-05	3.22E-05	-2.489722	0.0128
D11*TIME	2.43E-05	3.23E-05	0.753026	0.4514
D12*TIME	3.13E-05	2.92E-05	1.070849	0.2842
DTR_PHL(-1)	0.339047	0.007669	44.20912	0.0000

R-squared	0.190049	Mean dependent var		17.75151
Adjusted R-squared	0.189130	S.D. dependent var		6.461226
S.E. of regression	5.818225	Akaike info criterion		6.361047
Sum squared resid	716268.9	Schwarz criterion		6.370442
Log likelihood	-67351.21	Hannan-Quinn criter.		6.364112
F-statistic	206.8665	Durbin-Watson stat		1.997036
Prob(F-statistic)	0.000000	Wald F-statistic		149.6270
Prob(Wald F-statistic)	0.000000			

Figure A9: PHL Joint Conditional Variance Regression, AVG

Dependent Variable: E2_AVG_PHL
Method: Least Squares
Date: 07/09/19   Time: 13:46
Sample (adjusted): 1/03/1960 12/31/2017
Included observations: 21183 after adjustments
HAC standard errors & covariance (Bartlett kernel, Newey-West fixed
    bandwidth = 14.0000)

Variable	Coefficient	Std. Error	t-Statistic	Prob.
C	12.53425	0.856703	14.63081	0.0000
TIME	-8.55E-05	6.71E-05	-1.274025	0.2027
D1	27.95462	3.314398	8.434298	0.0000
D2	27.40326	3.694701	7.416908	0.0000
D3	19.65243	3.217091	6.108760	0.0000
D4	16.33077	2.814383	5.802609	0.0000
D5	15.64959	2.275583	6.877178	0.0000
D6	7.851489	1.614614	4.862766	0.0000
D8	1.684095	1.451363	1.160355	0.2459
D9	10.15016	1.696774	5.982032	0.0000
D10	15.41559	1.868326	8.251017	0.0000
D11	21.81678	2.580458	8.454616	0.0000
D12	25.32869	2.912196	8.697454	0.0000
D1*TIME	0.000147	0.000289	0.508400	0.6112
D2*TIME	2.29E-05	0.000311	0.073498	0.9414
D3*TIME	0.000468	0.000278	1.683618	0.0923
D4*TIME	0.000376	0.000229	1.646811	0.0996
D5*TIME	-0.000170	0.000170	-1.000579	0.3170
D6*TIME	-0.000154	0.000129	-1.191914	0.2333
D8*TIME	-0.000147	0.000104	-1.409849	0.1586
D9*TIME	-0.000204	0.000130	-1.572636	0.1158
D10*TIME	-0.000131	0.000150	-0.870783	0.3839
D11*TIME	-5.66E-05	0.000223	-0.253438	0.7999
D12*TIME	-0.000102	0.000226	-0.449544	0.6530
E2_AVG_PHL(-1)	0.045064	0.008634	5.219394	0.0000

R-squared	0.056834	Mean dependent var		28.65058
Adjusted R-squared	0.055765	S.D. dependent var		44.80583
S.E. of regression	43.53862	Akaike info criterion		10.38635
Sum squared resid	40107347	Schwarz criterion		10.39575
Log likelihood	-109982.1	Hannan-Quinn criter.		10.38942
F-statistic	53.12346	Durbin-Watson stat		2.002735
Prob(F-statistic)	0.000000	Wald F-statistic		71.11827
Prob(Wald F-statistic)	0.000000			

29

Figure A10: PHL Joint Conditional Variance Regression, DTR

Dependent Variable: E2_DTR_PHL
Method: Least Squares
Date: 07/09/19   Time: 13:46
Sample (adjusted): 1/03/1960 12/31/2017
Included observations: 21183 after adjustments
HAC standard errors & covariance (Bartlett kernel, Newey-West fixed
    bandwidth = 14.0000)

Variable	Coefficient	Std. Error	t-Statistic	Prob.
C	22.37441	2.025807	11.04469	0.0000
TIME	-0.000393	0.000143	-2.754483	0.0059
D1	10.66203	3.499646	3.046602	0.0023
D2	15.43329	3.251396	4.746665	0.0000
D3	23.89886	3.584542	6.667200	0.0000
D4	27.07562	3.612763	7.494436	0.0000
D5	23.21550	3.713078	6.252359	0.0000
D6	10.56819	2.869652	3.682741	0.0002
D8	-0.077822	2.467053	-0.031545	0.9748
D9	11.83351	3.131250	3.779164	0.0002
D10	15.76030	3.429174	4.595946	0.0000
D11	12.79291	3.141156	4.072675	0.0000
D12	11.53788	2.921364	3.949484	0.0001
D1*TIME	0.000435	0.000282	1.542890	0.1229
D2*TIME	0.000121	0.000256	0.471372	0.6374
D3*TIME	0.000287	0.000279	1.029384	0.3033
D4*TIME	0.000150	0.000283	0.531146	0.5953
D5*TIME	-0.000227	0.000269	-0.845246	0.3980
D6*TIME	-0.000307	0.000211	-1.455570	0.1455
D8*TIME	-9.88E-05	0.000176	-0.560119	0.5754
D9*TIME	-0.000565	0.000219	-2.586589	0.0097
D10*TIME	-0.000220	0.000244	-0.898320	0.3690
D11*TIME	0.000126	0.000236	0.535258	0.5925
D12*TIME	6.74E-05	0.000211	0.319497	0.7494
E2_DTR_PHL(-1)	0.067617	0.011837	5.712522	0.0000

R-squared	0.046411	Mean dependent var		33.80817
Adjusted R-squared	0.045329	S.D. dependent var		49.85206
S.E. of regression	48.70908	Akaike info criterion		10.61079
Sum squared resid	50198927	Schwarz criterion		10.62018
Log likelihood	-112359.2	Hannan-Quinn criter.		10.61385
F-statistic	42.90654	Durbin-Watson stat		2.001013
Prob(F-statistic)	0.000000	Wald F-statistic		56.51759
Prob(Wald F-statistic)	0.000000			